THE JOURNAL OF PHYSICAL CHEMISTRY A

Article

pubs.acs.org/JPCA

Vibrationally Resolved Photoelectron Spectroscopy of Electronic Excited States of DNA Bases: Application to the $\tilde{A}$ State of Thymine Cation

Majdi Hochlaf*

Laboratoire Modélisation et Simulation Multi Echelle, MSME UMR 8208 CNRS, Université Paris-Est, 5 bd Descartes, 77454 Marne-la-Vallée, France

Yi Pan and Kai-Chung Lau*

Department of Biology and Chemistry, City University of Hong Kong, Kowloon, Hong Kong

Youssef Majdi

Laboratoire de Spectroscopie Atomique, Moléculaire et Applications − LSAMA, Université de Tunis El Manar, Tunis, Tunisia

Lionel Poisson

Laboratoire Francis Perrin, CNRS URA 2453, CEA, IRAMIS, Laboratoire Interactions Dynamique et Lasers, , Bât 522, F-91191 Gif/Yvette, France

Gustavo A. Garcia and Laurent Nahon

Synchrotron SOLEIL, L'orme des Merisiers, Saint-Aubin - BP 48, 91192 Gif-sur-Yvette Cedex, France

Muneerah Mogren Al Mogren

Chemistry Department, Faculty of Science, King Saud University, P.O. Box 2455, Riyadh 11451, Kingdom of Saudi Arabia

Martin Schwell

Laboratoire Interuniversitaire des Systèmes Atmosphériques (LISA), UMR 7583 CNRS, Universités Paris-Est Créteil et Paris Diderot, Institut Pierre et Simon Laplace, 61 Avenue du Général de Gaulle, 94010 Créteil, France

S *Supporting Information*

ABSTRACT: For fully understanding the light−molecule interaction dynamics at short time scales, recent theoretical and experimental studies proved the importance of accurate characterizations not only of the ground (D0) but also of the electronic excited states (e.g., D1) of molecules. While ground state investigations are currently straightforward, those of electronic excited states are not. Here, we characterized the $\tilde{A}$ electronic state of ionic thymine (T^+) DNA base using explicitly correlated coupled cluster ab initio methods and state-of-the-art synchrotron-based electron/ion coincidence techniques. The experimental spectrum is composed of rich and long vibrational progressions corresponding to the population of the low frequency modes of $T^+(\tilde{A})$. This work challenges previous numerous works carried out on DNA bases using common synchrotron and VUV-based photoelectron spectroscopies. We provide hence a powerful theoretical and experimental framework to study the electronic structure of ionized DNA bases that could be generalized to other medium-sized biologically relevant systems.

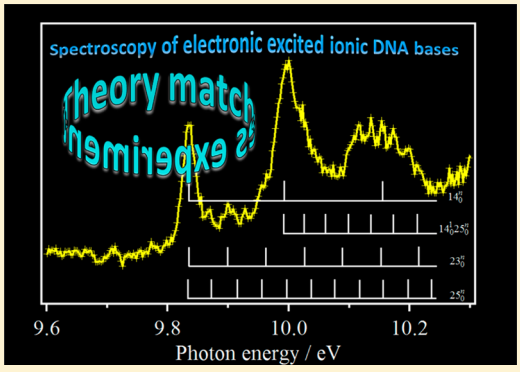

Received: January 16, 2015
Revised: January 21, 2015

DOI: 10.1021/acs.jpca.5b00466
J. Phys. Chem. A XXXX, XXX, XXX−XXX

I. INTRODUCTION

The control and prevention of the effects of ionization on biological molecules need knowledge about the excitation step, which in turn is based on the understanding of their structure and spectroscopy (both neutral and ionic forms), as well as the relaxation channels. For instance, the damages of ionizing radiation on DNA and RNA lead, at the microscopic level, to genetic mutations mediated by the generated ions, while the corresponding emitted photoelectrons will also contribute to further damages. For those purposes, the photoionization of DNA and RNA bases and analogues was widely studied experimentally and theoretically as recently reviewed by Schwell and Hochlaf.[1] However, vibrationally resolved photoelectron spectra of DNA/RNA bases are available only for the ground state of thymine cation (T^+).[1,2] For instance, the analysis of the highly resolved (fwhm ∼ 2 meV) mass-analyzed threshold ionization (MATI) spectrum of jet-cooled thymine[2] allowed determining an accurate adiabatic ionization energy (AIE) for $T^+(\tilde{X})$. The assignment of the observed vibrational structures was performed by a normal-mode analysis. The observed bands were attributed to the population of the low frequency modes ν^+_{27}, ν^+_{30}, ν^+_{33}, and ν^+_{39} of $T^+(\tilde{X})$. More recently, these assignments were confirmed by a more sophisticated theoretical treatment by Krylov and co-workers.[3]

Since the 1970s, numerous studies[2−9] have treated the VUV photoionization of thymine. For the electronic excited states of T^+, previous studies were, however, limited to the determination of their vertical ionization energies (VIE) and their electronic nature, and very little is known on their vibrational and equilibrium structures. In fact, the difficulties reside experimentally on the congestion of the spectra because of the overlap of several contributing bands and theoretically on the multiconfigurational nature of these electronic states and on the relatively large number of degrees of freedom for mapping the potential energy surfaces of such medium-sized molecular species. The determination of vibrational frequencies and molecular structure of excited T^+ states, and generally of DNA bases, remains a challenging task for both experimentalists and theoreticians.

In this work, we take advantage of synchrotron-based high resolution threshold photoelectron imaging techniques, in particular slow photoelectron spectroscopy (SPES),[10−12] to fully resolve the vibrational structure of the $T^+(\tilde{A})$ state. The rich structure observed in the experimental spectrum is assigned with the help of state-to-the-art ab initio post-Hartree−Fock computations on the structure and the spectroscopy of $T^+(\tilde{A})$. This work provides the experimental and theoretical framework for measuring and analyzing vibrationally resolved spectra of ionized DNA/RNA bases and, more generally, for medium-sized biologically relevant entities.

II. SPES SPECTRUM OF THE $T^+(\tilde{A})$ STATE

1. Experimental Methods. Experiments were performed at the DESIRS VUV undulator-based beamline[13] at the third generation, French synchrotron facility SOLEIL located in St Aubin, France. The experimental setup and procedure have already been described elsewhere[10−12,14] and are only briefly presented here. Pure solid thymine (Sigma-Aldrich) was vaporized inside a temperature controlled in-vacuum stainless steel CF oven heated at 200 °C. The vapor was mixed with 1 bar of He and expanded through a 50 μm nozzle, before traversing a 1 mm skimmer and entering the photoionization chamber where it crosses the synchrotron beam at a right angle. The produced photoelectrons and photoions were extracted perpendicularly and detected in coincidence using the DELICIOUS III spectrometer.[15] Velocity map imaging (VMI) photoelectron images for each mass are then recorded simultaneously and Abel inverted[16] to extract the photoelectron spectra with a 3.4 eV bandwidth. Note that the molecular beam was optimized so that no evidence of clusters—which could contribute to the thymine mass via dissociative photoionization—could be found either in the TOF or in the photoion images recorded (not shown here).

The synchrotron beamline was set to deliver 5×10^{12} photons/s with a 12 meV resolution at 10 eV. The light was linearly polarized with the electric vector contained in the spectrometer's detector plane, and the higher order radiation was removed by filling the upstream gas filter with 0.27 mbars of Ar.[17]

Scanning the monochromator yielded the electron intensity as a function of both kinetic energy and photon energy, called hereafter photoionization matrix. Due to energy conservation, direct processes appear as diagonal lines in the matrix having unity slope $KE = h\nu - IE_i$, where i is the ith state of the molecule having an ionization energy IE, and KE is the electron kinetic energy. Integrating the photoelectron signal along these diagonal lines yields the slow photoelectron spectrum, $SPES(h\nu) = \int_0^{KE_0} M(KE, h\nu + KE)\, dKE$,[10] where M is the intensity matrix (cf. Figure 1). The SPES is equivalent to the more common

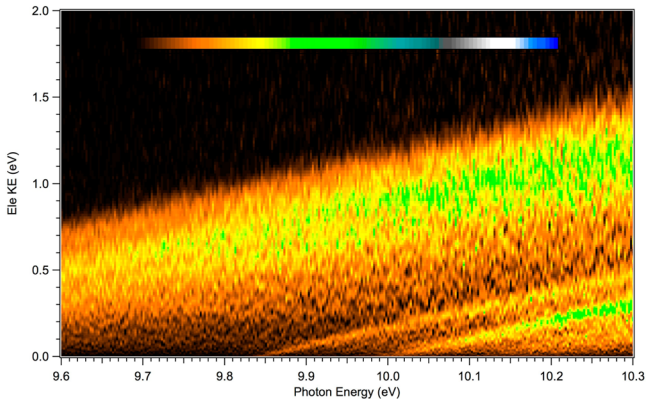

Figure 1. Photoionization intensity matrix tracing the electron signal as a function of the electron and photon energy (see ref 10), in the region of the $T^+(\tilde{A})$ state.

threshold photoelectron spectrum, except that it uses electrons having KE up to KE_0, instead of only threshold electrons, dramatically increasing the signal-to-noise ratio without any important loss in resolution, provided that the electrons are kept slow enough so that the degrading VMI resolution does not affect the overall resolution.

The energy calibration of the bands is based on the 4s and 4s′ absorption lines of Ar[18] (in the gas filter) and not something inside the interaction region. Therefore, we corrected the initial band positions for the Stark shift. The inhomogeneous field has been calculated in the center of the ionization region by solving the Laplace equation for our geometry. It gives a value of E = 88 V/cm (E is the electric field). Applying the 6*sqrt(E) formula to calculate the Stark Shift, we obtain an offset of 7 meV. In the following, we present the corrected band origins.

2. Presentation of the 2D and 1D SPES Spectrum of the $T^+(\tilde{A})$ State. On the basis of previous theoretical and experimental studies,[19−22] only the most stable form of thymine (i.e., the *cis*-diketo structure) is expected to be present in the molecular beam prior to photoionization. Moreover, the cooling

DOI: 10.1021/acs.jpca.5b00466
J. Phys. Chem. A XXXX, XXX, XXX−XXX

ensures that hot vibrational bands should be quasi-absent in the experimental spectra.

The photoionization intensity matrix describing the electron signal as a function of its kinetic energy and of the photon energy in the $h\nu$ = 9.6−10.3 eV energy range is shown in Figure 1. Inspection of this figure reveals that the photoionization of T occurs mainly via a direct process in the 9.6−10.3 eV energy range, with no visible autoionization contribution that would appear as vertically aligned features in Figure 1.

Figure 2 displays the one-dimensional SPES extracted from the ionization matrix, for different electron energy limits

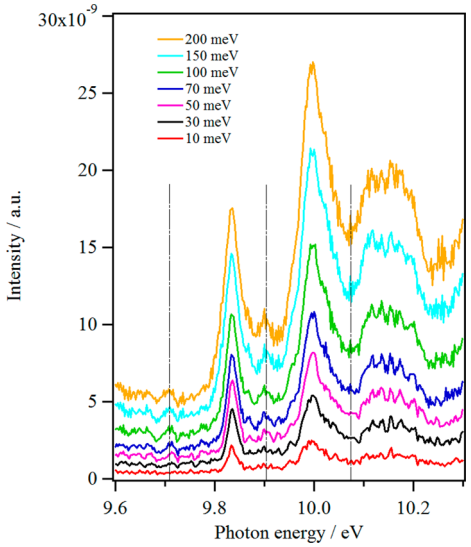

Figure 2. Slow photoelectron spectra (SPES) deduced from the 2D spectrum (Figure 1) by considering photoelectrons having kinetic energies (KE_0) from 0 to 10 meV, 0 to 30 meV, 0 to 50 meV, 0 to 70 meV, 0 to 100 meV, 0 to 150 meV, and 0 to 200 meV.

KE_0 = 10, 30, 50, 70, 100, 150, and 200 meV. As established in refs 10−12, such a procedure ensures better statistics with only slight perturbation in the overall full width at half-maximum (fwhm) of the bands. This is clearly evidenced in Figure 2. Indeed, the threshold photoelectron spectrum (TPES, i.e. KE_0 = 10 meV) is noisy, and only the strong features relative to the vibrational bands of $T^+(\tilde{A})$ can be seen there. In contrast, the SPES spectra with $KE_0 \geq 30$ meV show clearly the appearance of weak bands (e.g., those highlighted by vertical dashed-dotted lines in Figure 2), which are also due to the vibrational structure of this ion (see below). Importantly, the set of bands between 10.08 and 10.25 eV, which correspond to the real vibrational structure of $T^+(\tilde{A})$, are missing from the TPES spectrum. Indeed, if we integrate more along the bright lines of Figure 1, resonant autoionization will be washed out. And if autoionization appears, the shape of the SPES spectrum would change, which is not the case at present. Such a procedure allowed us also to check data for artifacts. Moreover, Figure 2 shows that the branching ratios between the different peaks do not change when faster electrons (different photon energies) are allowed into the treatment. Assuming flat differential cross sections, this fact indicates that resonant autoionization is not present in our SPES.[12] Since all ratios remained almost unchanged for different KE_0, we could conclude that the small bands are real and no autoionization is observed. Incidentally, Figure 2 also helps to identify the real bands with respect to experimental noise.

When comparing our spectra with the photoelectron spectrum (PES) of Trofimov et al.,[9] with the photoion efficiency (PIE) spectrum, or with the PES spectrum obtained by differentiating the corresponding PIE spectrum (dPIE/dE curve) by Bravaya et al.,[3] the present SPES spectrum shows richer structures which were not found in previous studies.[3,9] This highlights the capabilities of the SPES technique in connection with VUV-synchrotron to routinely record and probe the spectra of electronically excited states of ionized DNA bases. It also shows that the approach of differentiating the PIE curves to obtain photoelectron spectra is too simplistic since the experimental noise on the PIE curves and the possible presence of indirect processes preclude this mathematical operation.

III. EQUILIBRIUM GEOMETRY AND THEORETICAL SPECTROSCOPY OF THE $T^+(\tilde{A})$ STATE

In the literature, only the VIE of the $\tilde{A}$ state is known. VIE corresponds to the difference between the energies of $T(\tilde{X})$ and $T^+(\tilde{A})$ taken at the equilibrium geometry of $T(\tilde{X})$. This quantity may not be, however, adequate for the assignment of the present vibrationally revolved spectrum. Therefore, we performed a geometry optimization and frequency computation for $T^+(\tilde{A})$ using the complete active-space self-consistent field (CASSCF)[23,24] technique and the aug-cc-pVDZ basis set of Dunning and co-workers.[25,26] These computations were done using the MOLPRO suite of programs.[27]

The geometry optimizations were done in the C_1 point group, where we used the default options. At the state-averaged CASSCF (SA-CASSCF), two cation states [$T^+(\tilde{X})$ and $T^+(\tilde{A})$] were included. The active space is constructed using 10 molecular orbitals from HOMO−4 up to LUMO+4. During the CASSCF calculations, the 9 core orbitals and the first 19 valence orbitals (up to HOMO−5) were kept as closed orbitals. The results are given in Tables 1 and 2.

Similar to the neutral ground state of thymine, the first excited ($\tilde{A}$) state of the thymine cation possesses a cis planar equilibrium geometry. The trans form is a transition state (see Tables S1−**S3** of the Supporting Information) and both the cis and the trans are of $^2A'$ group symmetry. Cis/trans isomerization corresponds to the rotation of the methyl group. $T^+(\tilde{A})$ is formed after ejection of an electron from the outermost a′ molecular orbital (MO) of thymine. Following the analysis of previous studies,[3,9] this MO is part of the σ system, and it involves the lone pair of O and the CO bonds (i.e., σ_{LP-O}). Ionization-induced structural changes are hence expected upon the $T(\tilde{X}) + h\nu \rightarrow T^+(\tilde{A}) + e^-$ transition. This is confirmed by the analysis of the equilibrium geometries (Table 1 and Figure 3) of $T(\tilde{X})$[28] and $T^+(\tilde{A})$. For instance, the main difference between both species occurs around the C_4 atom: the C_4-O_8 bond of the cation is much longer than that in the neutral (by ∼0.09 Å) and the N_3-C_4 and C_4-C_5 bonds are differed by ∼0.07−0.09 Å. In a lesser way the C_6-N_1 is also affected upon photoionization. One can see also that the $C_2-N_3-C_4$, $N_3-C_4-C_5$, $C_4-C_5-C_6$, $N_3-C_4-O_8$, and $C_4-C_5-C_9$ in-plane angles differ from their corresponding neutral values by more than ∼5°.

IV. SPECTROSCOPY OF $T^+(\tilde{A}^2A')$

On the basis of the Franck−Condon principle, different modes, especially those involving the CO bonds and their neighboring internal coordinates, are expected to be populated when forming the $\tilde{A}$ state of T^+ by photoionizing $T(\tilde{X})$, which should result in long vibrational progressions. The computed anharmonic

DOI: 10.1021/acs.jpca.5b00466
J. Phys. Chem. A XXXX, XXX, XXX−XXX

Table 1. Main Geometrical Parameters (Å and deg) of the Ground State of Neutral *cis*-Thymine [$T(\tilde{X}^1A')$] and of the First Excited State of *cis*-Thymine Cation [$T^+(\tilde{A}^2A')$]

	$T(\tilde{X}^1A')^a$	$T^+(\tilde{A}^2A')^b$
N_1-C_2	1.396	1.394
C_2-N_3	1.394	1.391
N_3-C_4	1.413	1.344
C_4-C_5	1.469	1.376
C_5-C_6	1.368	1.379
C_6-N_1	1.383	1.330
C_2-O_7	1.228	1.200
C_4-O_8	1.235	1.329
C_5-C_9	1.502	1.516
N_1-H_{10}	1.016	1.001
N_3-H_{11}	1.021	1.002
C_6-H_{12}	1.095	1.078
C_9-H_{13}	1.103	1.086
C_9-H_{14}	1.103	1.086
C_9-H_{15}	1.102	1.085
$N_1-C_2-N_3$	112.0	112.4
$C_2-N_3-C_4$	129.0	122.9
$N_3-C_4-C_5$	114.0	124.1
$C_4-C_5-C_6$	118.5	113.1
$C_5-C_6-N_1$	122.5	123.5
$N_3-C_2-O_7$	124.6	123.9
$N_3-C_4-O_8$	120.9	114.1
$C_4-C_5-C_9$	117.6	122.9

[a]CC2/TVZP. Reference 28. [b]Optimized at SA-CASSCF/aug-cc-pVDZ level of theory.

frequencies for the $T^+(\tilde{A})$ state are listed in Table 2 together with their identification in terms of normal modes. According to previous works on similar systems,[29,30] these values should be accurate within 20−30 cm^{-1}, which is likely sufficient for the assignment of the present vibrationally resolved experimental spectrum.

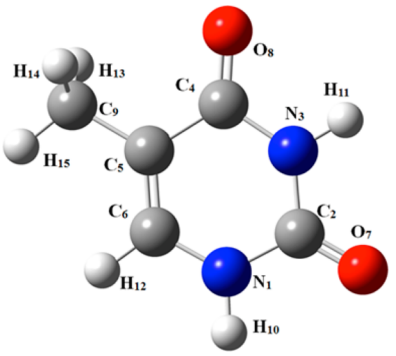

Figure 3. Numbering of the atoms used in the present work.

In the energy range 9.6−10.3 eV, the high vibrational levels of $T^+(\tilde{X})$ and the vibrational levels of $T^+(\tilde{A})$ are expected to be populated. The bands in Figures 2 and 4 are due to the formation of T^+ cation since no fragmentation is expected below 10.7 eV.[8] In the following, we propose a tentative assignment of these vibrational features based on our theoretical results. Our analyses were guided by the anharmonic frequencies and the decomposition of the corresponding normal modes on the corresponding internal coordinates as presented in Table 2. This assignment is given in Figure 4.

1. Adiabatic Ionization Energy. The calculated AIE of $T^+(\tilde{A})$ is a sum of two parts: (i) the adiabatic IE of thymine obtained at the CCSD(T)-F12(b)/cc-pVTZ-F12 level[31] and (ii) energy difference between $T^+(\tilde{X})$ and $T^+(\tilde{A})$ at their respective equilibrium geometries. The second part of the contribution to AIE of $T^+(\tilde{A})$ has been computed at different levels of theory (Table 3). At the SA-CASSCF/aug-cc-pVDZ level, the AIE of $T^+(\tilde{A})$ is calculated to be 10.017 eV. For better accuracy, we

Table 2. Anharmonic Frequencies (ν, in cm^{-1}) of the First Excited State ($\tilde{A}^2A'$) of *cis*-Thymine$^+$, Obtained at SA-CASSCF/aug-cc-pVDZ Level of Theory[a]

no.	symmetry	ν	assignment	no.	symmetry	ν	assignment
1	a′	3454	ν NH	21	a′	730	δ ring
2	a′	3437	ν NH	22	a′	556	δ ring, β CH
3	a′	3056	ν CH	23	a′	502	$\delta(N_3C_2O_7)$, $\delta(N_3C_4O_8)$
4	a′	2973	ν CH	24	a′	452	δ ring, β CH
5	a′	2896	ν CH	25	a′	338	$\delta(N_3C_2O_7)$, $\delta(N_3C_4O_8)$
6	a′	1743	$\nu(C_2O_7)$, β NH	26	a′	250	$\delta(C_4C_5C_9)$
7	a′	1641	$\nu(C_4C_5)$, β NH	27	a″	2963	ω CH
8	a′	1603	$\nu(C_5C_6)$, β CH	28	a″	1455	γ CH
9	a′	1503	β NH, δ ring	29	a″	1075	γ CH
10	a′	1467	β CH	30	a″	1018	γ CH
11	a′	1433	β NH, δ ring	31	a″	729	τ ring
12	a′	1411	β CH, β NH	32	a″	703	γ NH, γ CH
13	a′	1310	β NH, δ ring	33	a″	656	γ NH, γ CH
14	a′	1284	$\nu(C_4O_8)$, β CH	34	a″	578	γ NH, γ CH
15	a′	1217	δ ring, β NH	35	a″	403	γ CH, τ ring
16	a′	1175	δ ring, β CH	36	a″	274	τ ring, γ CH
17	a′	1043	δ ring, β NH	37	a″	195	τ ring
18	a′	975	β CH, δ ring	38	a″	112	τ ($-CH_3$ group)
19	a′	925	δ ring, β CH	39	a″	97	τ ($-CH_3$ group)
20	a′	760	δ ring, β NH				

[a]In plane vibration: ν stretching, β bending, δ deformation. Out of plane vibration: γ wagging, ω anti-symmetry stretching, τ torsion. The anharmonic frequencies are obtained after scaling the corresponding harmonic vibrational frequencies by 0.91 (see ref 29). These frequencies are given in a descending order under a′ symmetry (in-plane vibrations) and a″ symmetry (out-of-plane vibrations).

DOI: 10.1021/acs.jpca.5b00466
J. Phys. Chem. A XXXX, XXX, XXX−XXX

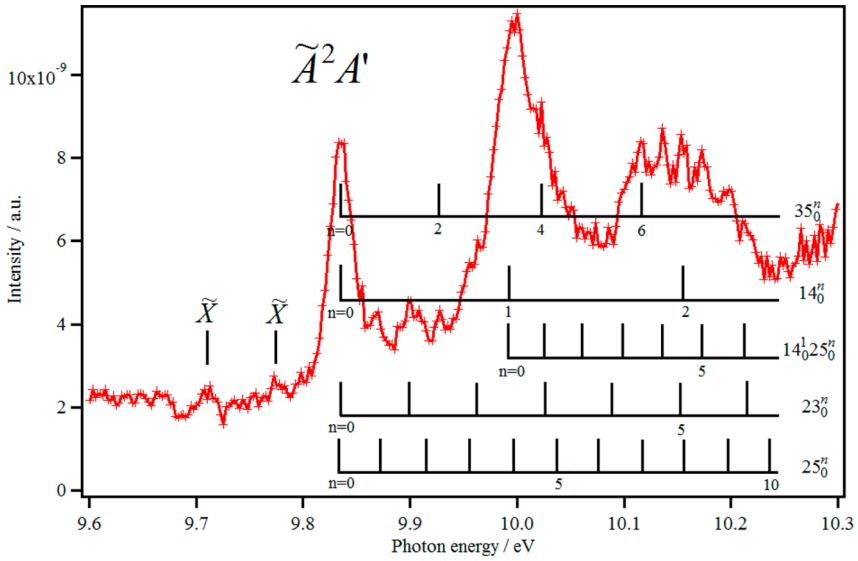

Figure 4. SPES spectrum of Figure 2 (cf. Table S4 of Supporting Information), where we considered the photoelectrons with kinetic energies from 0 to KE_0 = 70 meV. This yields an electron energy resolution of 20 meV. Comb lines correspond to the tentative assignments. The peaks marked by "$\tilde{X}$" are vibrational progressions contributed by $T^+(\tilde{X})$.

Table 3. AIE of $T^+(\tilde{A})$ Computed at Different Levels of Theory[a]

method	AIE, eV
Calc. SA-CASSCF/aug-cc-pVDZ[b]	10.017
Calc. MRCI/aug-cc-pVDZ[c]	9.981
Calc. MRCI+Q/aug-cc-pVDZ[d]	9.969
Calc. CCSD(T)-F12(b)/cc-pVTZ-F12 (+CV+SR+ZPVE)[b]	**9.868**
Exp. SPES[b]	**9.842 ± 0.005**
Calc. CASPT2(IPEA = 0.25)//CASSCF/ANO-L 431/21[e,f]	9.81
Calc. EOM-IP-CCSD/cc-pVTZ//RI-MP2/cc-pVTZ[e,g]	10.13
Exp. PES[e,h]	10.14

[a]We also give the values deduced from the SPES spectrum of Figures 2 and 4 together with their comparison with previous determinations. The experimental and preferred theoretical values obtained in this work are written in bold. [b]This work. AIE$[T^+(\tilde{A})]$ = AIE(T) + E$[T^+(\tilde{A}) - T^+(\tilde{X})]$; see text for details. [c]Single point computations at the SA-CASSCF optimized geometry. [d]Single point computations at the SA-CASSCF optimized geometry and including Davidson correction. [e]VIE. [f]Reference 48. [g]Reference 3. [h]Reference 9.

performed single point computations on the SA-CASSCF equilibrium geometries of $T^+(\tilde{X})$ and of $T^+(\tilde{A})$ using the internally contracted multireference configuration interaction technique (MRCI)[32,33] with and without including the Davidson correction.[34] In these calculations, all 9 core orbitals and first 17 valence orbitals were kept frozen. The calculated AIEs are 9.981 (MRCI/aug-cc-pVDZ) and 9.969 eV (MRCI+Q/aug-cc-pVDZ).

In addition, we took advantage of the newly implemented explicitly correlated coupled cluster approach to compute the AIE of $T^+(\tilde{A})$. We used hence the (R)CCSD(T)-F12 (approximation b) method[35−37] in connection with the cc-pVTZ-F12 explicitly correlated basis sets[38] and the corresponding auxiliary basis sets and density fitting functions.[39−42] Then, we included the core−valence (CV, as the difference between CCSD(T)/cc-pwCVTZ energies with and without considering core electrons),[43,44] scalar-relativistic (SR, as the difference between CCSD(T)/cc-pVTZ-DK and CCSD(T)/cc-pVTZ energies),[45−47] and zero point vibrational energy (ZPVE) corrections. At the CCSD(T)-F12(b) (+CV+SR+ZPVE) level, we deduce hence an AIE$[T^+(\tilde{A})]$ of 9.868 eV for the *cis* form. The theoretical AIE at the CCSD(T)-F12(b) (+CV+SR+ZPVE) level coincides with the first strong peak in the SPES spectrum of Figures 2 and 4. The experimental AIE is therefore determined at 9.842 ± 0.005 eV. This value agrees with the computations of Roca-Sanjuán et al.[48] but is distinctly lower than the previously determined VIEs (see Table 3 for more details).

At the CCSD(T)-F12(b) (+CV+SR+ZPVE) level, we deduce an AIE$[trans\text{-}T^+(\tilde{A})]$ 43 meV higher than the cis form. These costly computations confirm the trans form is a transition state (Supporting Information Table S1). Therefore, the *trans* form is unlikely to contribute any photoelectron signal to the experimental spectrum.

2. Tentative Assignment. Both *cis*-$T(\tilde{X})$ and *cis*-$T^+(\tilde{A})$ species are planar. Upon single photon ionization, only vibrational bands of a′ symmetry are allowed. This corresponds to cationic a′ mode excitations and to the even overtones and combinations of a″ vibrational modes. We propose in Figure 4 and Table 4 a tentative assignment of these bands, where we fully attribute the spectrum with three pure vibration progressions involving modes 23 (i.e., 23_0^n series, n = 0−6), 25 (25_0^n series, n = 0−10), and 14 (i.e., 14_0^n series, n = 0−2), a combination mode ($14_0^1 25_0^n$ for n = 0−6), and even overtones of mode 35. The corresponding theoretically obtained vibrational transition energies match very well the observed vibrational structures visible on the SPES. For mode 23, we measure a spacing of ∼65 meV (∼520 cm^{-1}), which is close to the anharmonic frequency (of 502 cm^{-1}) computed for this mode (Table 4). For the 25_0^n progression, we have a spacing of ∼35 meV (∼282 cm^{-1}),

DOI: 10.1021/acs.jpca.5b00466
J. Phys. Chem. A XXXX, XXX, XXX−XXX

Table 4. Tentative Assignment for the Observed Bands from the SPES Spectrum of Figure 4

tentative assignment	observed energy, eV	observed frequencies,[a] cm^{-1}	calculated frequencies, cm^{-1}
$\tilde{A}0_0^0$	9.842	0	
$\tilde{A}25_0^1$	9.877	282	338
$\tilde{A}23_0^1$	9.907	524	502
$\tilde{A}25_0^2$	9.915	589	676
$\tilde{A}35_0^2$	9.935	750	806
$\tilde{A}25_0^3$	9.963	976	1014
$\tilde{A}23_0^2$	9.970	1032	1004
$\tilde{A}14_0^1$	10.002	1290	1284
$\tilde{A}25_0^4$	10.008	1339	1352
$\tilde{A}35_0^4$	10.030	1516	1612
$\tilde{A}23_0^3$ or $\tilde{A}14_0^125_0^1$	10.035	1557	1506 or 1622
$\tilde{A}25_0^5$	10.050	1678	1690
$\tilde{A}14_0^125_0^2$	10.065	1799	1960
$\tilde{A}25_0^6$	10.073	1863	2028
$\tilde{A}23_0^4$	10.080	1920	2008
$\tilde{A}14_0^125_0^3$	10.093	2024	2298
$\tilde{A}25_0^7$	10.115	2202	2366
$\tilde{A}35_0^6$	10.123	2266	2418
$\tilde{A}14_0^125_0^4$	10.143	2428	2636
$\tilde{A}23_0^5$	10.153	2508	2510
$\tilde{A}14_0^2$	10.160	2565	2568
$\tilde{A}25_0^8$	10.165	2605	2704
$\tilde{A}14_0^125_0^5$	10.180	2726	2974
$\tilde{A}25_0^9$	10.205	2928	3042
$\tilde{A}23_0^6$ or $\tilde{A}14_0^125_0^6$	10.218	3033	3012 or 3312

[a]Relative to the origin band of $T^+(\tilde{A})$.

which is consistent with the calculated ν_{25}^+ frequency (of 338 cm^{-1}, Table 4). We measure also the experimental frequency to be ν_{14}^+ = 1290 cm^{-1}, which is close to the theoretical value of 1284 cm^{-1} (Table 4). The computed anharmonic frequency for mode 35 (~400 cm^{-1}) agrees with the 750 cm^{-1} spacing measured for two quanta of this mode. All these normal modes involve C_4-O_8 stretching and $N_3-C_4-O_8$ in-plane angular deformations, which is consistent with the major geometrical differences between $T(\tilde{X})$ and $T^+(\tilde{A})$ as noticed above.

Note that the relative intensities of the bands are not regular because of the "accidental" contribution of several vibrational bands. Simple Franck–Condon analysis cannot predict such irregularities.

V. CONCLUSIONS

In this combined theoretical and experimental treatment, we characterized the vibrational structure of the first electronically excited state of the T^+ cation. The well-resolved rich and complex features correspond to the population of relatively low frequency modes of the cation and the combination modes having large changes in the equilibrium structures between $T(\tilde{X})$ and $T^+(\tilde{A})$. The relative intensities do not adhere to simple Franck–Condon envelopes which invalidates the use of such approaches for the prediction of photoelectron spectra of T and more generally of DNA/RNA bases and biological molecular species.

Specifically, the present work points out the outstanding capabilities of explicitly correlated CCSD(T)-F12(b)/cc-pVTZ-F12 (+CV+SR+ZPVE) technique for predicting accurate energetics and of the coincident imaging SPES method in connection with a VUV high-brilliance synchrotron source for characterizing the electronic excited states of this class of molecules. This is for instance relevant for the understanding of the interaction between ionizing radiation and biological macromolecules as stressed in the introduction and, furthermore, for an in-depth understanding of the underlying mechanisms in ultrafast dynamics of DNA and RNA bases as pointed out in these recent theoretical and experimental investigations.[49−51]

■ ASSOCIATED CONTENT

Supporting Information

The full lists of coauthors for refs 10, 27, and 50 are provided. We give also energies of the cis- and trans- forms of $[T^+(\tilde{A}^2A')]$ at SA-CASSCF and MP2 levels (Table S1), main geometrical parameters (Table S2), anharmonic frequencies (Table S3), and the main results on the *trans* form of $T^+(\tilde{A})$ and 1D raw (Table S4) spectra of thymine in the 9.6−10.3 eV energy domain. This material is available free of charge via the Internet at http://pubs.acs.org.

■ AUTHOR INFORMATION

Corresponding Authors

*M. Hochlaf: tel. +33160957319; fax +33160957320; e-mail hochlaf@univ-mlv.fr.

*K.-C. Lau: tel. +85234426849; fax +85234420522; e-mail kaichung@cityu.edu.hk.

Notes

The authors declare no competing financial interest.

■ ACKNOWLEDGMENTS

This study was undertaken while M.H. was a Visiting Professor at King Saud University. The support of the Visiting Professor Program at King Saud University is hereby gratefully acknowledged. We acknowledge Marie Curie International Research Staff Exchange Scheme Fellowship within the 7th European Community Framework Program under Grant No. PIRSES-GA-2012-31754 and COST ACTION CM1405 MOLIM. Parts of the theoretical work were supported by the Research Grants Council of Hong Kong (CityU 101512). We are indebted to the general technical staff of Synchrotron Soleil for running the facility and providing beamtime under Project No. 20131221. We would like also to thank Jean-François Gil for his technical help on the SAPHIRS molecular beam chamber as well as a financial support from the French National program *Physique et Chimie du Milieu Interstellaire* PCMI (INSU, CNRS).

■ REFERENCES

(1) Schwell, M.; Hochlaf, M. Photoionization Spectroscopy of Nucleobases and Analogues in the Gas Phase Using Synchrotron Radiation as Excitation Light Source. *Topics of Current Chemistry*; Springer-Verlag: Berlin, Heidelberg, 2014.

(2) Choi, K. W.; Lee, J. H.; Kim, S. K. Ionization Spectroscopy of a DNA Base: Vacuum-Ultraviolet Mass-Analyzed Threshold Ionization Spectroscopy of Jet-Cooled Thymine. *J. Am. Chem. Soc.* **2005**, *127*, 15674−15675.

(3) Bravaya, K. B.; Kostko, O.; Dolgikh, S.; Landau, A.; Ahmed, M.; Krylov, A. I. Electronic Structure and Spectroscopy of Nucleic Acid Bases: Ionization Energies, Ionization-Induced Structural Changes, and Photoelectron Spectra. *J. Phys. Chem. A* **2010**, *114*, 12305−12317.

(4) Lauer, G.; Schäfer, W.; Schweig, A. Functional Subunits in the Nucleic Acid Bases Uracil and Thymine. *Tetrahedron Lett.* **1975**, *16*, 3939−3942.

(5) Dougherty, D.; Wittel, K.; Meeks, J.; McGlynn, S. P. Photoelectron Spectroscopy of Carbonyls. Ureas, uracils, and thymine. *J. Am. Chem. Soc.* **1976**, *98*, 3815−3820.

DOI: 10.1021/acs.jpca.5b00466
J. Phys. Chem. A XXXX, XXX, XXX−XXX

(6) Padva, A.; O'Donnell, T. J.; LeBreton, P. R. UV Photoelectron Studies of Biological Pyrimidines: the Valence Electronic Structure of Methyl Substituted Uracils. *Chem. Phys. Lett.* **1976**, *41*, 278−282.
(7) Urano, S.; Yang, X.; LeBreton, P. R. UV Photoelectron and Quantum Mechanical Characterization of DNA and RNA Bases: Valence Electronic Structures of Adenine, 1,9-Dimethyl-guanine, 1-Methylcytosine, Thymine and Uracil. *J. Mol. Struct.* **1989**, *214*, 315−328.
(8) Jochims, H. W.; Schwell, M.; Baumgärtel, H.; Leach, S. Photoion Mass Spectrometry of Adenine, Thymine and Uracil in the 6−22 eV Photon Energy Range. *Chem. Phys.* **2005**, *314*, 263−282.
(9) Trofimov, A. B.; Schirmer, J.; Kobychev, V. B.; Potts, A. W.; Holland, D. M. P.; Karlsson, L. Photoelectron Spectra of the Nucleobases Cytosine, Thymine and Adenine. *J. Phys. B: At. Mol. Opt. Phys.* **2006**, *39*, 305−329.
(10) Poully, J. C.; Schermann, J. P.; Nieuwjaer, N.; Lecomte, F.; Grégoire, G.; Desfrançois, C.; Garcia, G. A.; Nahon, L.; Nandi, D.; Poisson, L.; et al. Photoionization of 2-Pyridone and 2-Hydroxypyridine. *Phys. Chem. Chem. Phys.* **2010**, *12*, 3566−3572.
(11) Mahjoub, A.; Hochlaf, M.; Poisson, L.; Nieuwjaer, N.; Lecomte, F.; Schermann, J. P.; Grégoire, G.; Manil, B.; Garcia, G. A.; Nahon, L. Slow Photoelectron Spectroscopy of δ-Valerolactam and Its Dimer. *ChemPhysChem* **2011**, *12*, 1822−1832.
(12) Briant, M.; Poisson, L.; Hochlaf, M.; de Pujo, P.; Gaveau, M.-A.; Soep, B. Ar_2 Photoelectron Spectroscopy Mediated by Autoionizing States. *Phys. Rev. Lett.* **2012**, *109*, 193401.
(13) Nahon, L.; de Oliveira, N.; Garcia, G. A.; Gil, J.-F.; Pilette, B.; Marcouillé, O.; Lagarde, B.; Polack, F. DESIRS: A State-of-the-Art VUV Beamline Featuring High Resolution and Variable Polarization for Spectroscopy and Dichroism at SOLEIL. *J. Synchrotron Radiat.* **2012**, *19*, 508−520.
(14) Pan, Y.; Lau, K.-C.; Poisson, L.; Garcia, G. A.; Nahon, L.; Hochlaf, M. Slow Photoelectron Spectroscopy of 3-Hydroxyisoquinoline. *J. Phys. Chem. A* **2013**, *117*, 8095−8102.
(15) Garcia, G. A.; de Miranda, B. K. C.; Tia, M.; Daly, S.; Nahon, L. DELICIOUS III: A Multipurpose Double Imaging Particle Coincidence Spectrometer for Gas Phase Vacuum Ultraviolet Photodynamics Studies. *Rev. Sci. Instrum.* **2013**, *84*, 053112.
(16) Garcia, G. A.; Nahon, L.; Powis, I. Two-Dimensional Charged Particle Image Inversion using a Polar Basis Function Expansion. *Rev. Sci. Instrum.* **2004**, *75*, 4989−4996.
(17) Mercier, B.; Compin, M.; Prevost, C.; Bellec, G.; Thissen, R.; Dutuit, O.; Nahon, L. Experimental and Theoretical Study of a Differentially Pumped Absorption Gas Cell used as a Low Energy-pass Filter in the Vacuum Ultraviolet Photon Energy Range. *J. Vac. Sci. Technol. A* **2000**, *18*, 2533−2541.
(18) Yoshino, K. Absorption Spectrum of the Argon Atom in the Vacuum-Ultraviolet Region. *J. Opt. Soc. Am.* **1970**, *60*, 1220−1229.
(19) Rejnek, J.; Hanus, M.; Kabeláč, M.; Ryjáček, F.; Hobza, P. Correlated *ab initio* Study of Nucleic Acid Bases and Their Tautomers in the Gas Phase, in a Microhydrated Environment and in Aqueous Solution. Part 4. Uracil and Thymine. *Phys. Chem. Chem. Phys.* **2005**, *7*, 2006−2017.
(20) Colarusso, P.; Zhang, K. Q.; Guo, B.; Bernath, P. F. The Infrared Spectra of Uracil, Thymine, and Adenine in the Gas Phase. *Chem. Phys. Lett.* **1997**, *269*, 39−48.
(21) Brown, R. D.; Godfrey, P. D.; McNaughton, D.; Pierlot, A. P. Microwave Spectrum of the Major Gas-phase Tautomer of Thymine. *J. Chem. Soc., Chem. Commun.* **1989**, *1*, 37−38.
(22) Dolgounitcheva, O.; Zakrzewski, V. G.; Ortiz, J. V. Ionization Energies and Dyson Orbitals of Thymine and Other Methylated Uracils. *J. Phys. Chem. A* **2002**, *106*, 8411−8416.
(23) Knowles, P. J.; Werner, H.-J. An Efficient Second-order MC SCF Method for Long Configuration Expansions. *Chem. Phys. Lett.* **1985**, *115*, 259−267.
(24) Werner, H.-J.; Knowles, P. J. A Second Order Multiconfiguration SCF Procedure with Optimum Convergence. *J. Chem. Phys.* **1985**, *82*, 5053−5063.
(25) Dunning, T. H. Gaussian Basis Sets for Use in Correlated Molecular Calculations. I. The Atoms Boron through Neon and Hydrogen. *J. Chem. Phys.* **1989**, *90*, 1007−1023.
(26) Kendall, R. A.; Dunning, T. H.; Harrison, R. J. Electron Affinities of the First-Row Atoms Revisited. Systematic Basis Sets and Wave Functions. *J. Chem. Phys.* **1992**, *96*, 6796−6806.
(27) Werner, H.-J.; Knowles, P. J.; Knizia, G.; Manby, F. R.; Schütz, M.; Celani, P.; Korona, T.; Lindh, R.; Mitrushenkov, A.; Rauhut, G.; et al. *MOLPRO*, a package of ab initio programs. See http://www.molpro.net.
(28) Etinski, M.; Fleig, T.; Marian, C. M. Intersystem Crossing and Characterization of Dark States in the Pyrimidine Nucleobases Uracil, Thymine, and 1-Methylthymine. *J. Phys. Chem. A* **2009**, *113*, 11809−11816.
(29) Gagliardi, L.; Orlandi, G.; Bernardi, F.; Cembran, A.; Garavelli, M. A Theoretical Study of the Lowest Electronic States of Azobenzene: The Role of Torsion Coordinate in the Cis−trans Photoisomerization. *Theor. Chem. Acc.* **2004**, *111*, 363−372.
(30) Pan, Y.; Lau, K.-C.; Al-Mogren, M. M.; Mahjoub, A.; Hochlaf, M. Theoretical Studies of 2-Quinolinol: Geometries, Vibrational Frequencies, Isomerization, Tautomerism, and Excited States. *Chem. Phys. Lett.* **2014**, *613*, 29−33.
(31) Majdi, Y.; Hochlaf, M.; Pan, Y.; Lau, K.-C.; Poisson, L.; Garcia, G. A.; Nahon, L.; Al-Mogren, M. M.; Schwell, M. Theoretical and Experimental Photoelectron Spectroscopy Characterization of the Ground State of Thymine Cation. *J. Phys. Chem. A* **2015**, DOI: 10.1021/jp510716c.
(32) Werner, H.-J.; Knowles, P. J. An Efficient Internally Contracted Multiconfiguration−Reference Configuration Interaction Method. *J. Chem. Phys.* **1988**, *89*, 5803−5814.
(33) Knowles, P. J.; Werner, H.-J. An Efficient Method for the Evaluation of Coupling Coefficients in Configuration Interaction Calculations. *Chem. Phys. Lett.* **1988**, *145*, 514−522.
(34) Langhoff, S. R.; Davidson, E. R. Configuration Interaction Calculations on the Nitrogen Molecule. *Int. J. Quantum Chem.* **1974**, *8*, 61−72.
(35) Adler, T. B.; Knizia, G.; Werner, H.-J. A Simple and Efficient CCSD(T)-F12 Approximation. *J. Chem. Phys.* **2007**, *127*, 221106.
(36) Werner, H.-J.; Knizia, G.; Manby, F. R. Explicitly Correlated Coupled Cluster Methods with Pair-specific Geminals. *Mol. Phys.* **2011**, *109*, 407−417.
(37) Knizia, G.; Adler, T. B.; Werner, H.-J. Simplified CCSD(T)-F12 Methods: Theory and Benchmarks. *J. Chem. Phys.* **2009**, *130*, 054104.
(38) Peterson, K. A.; Adler, T. B.; Werner, H.-J. Systematically Convergent Basis Sets for Explicitly Correlated Wavefunctions: The Atoms H, He, B−Ne, and Al−Ar. *J. Chem. Phys.* **2008**, *128*, 084102.
(39) Weigend, F. A Fully Direct RI-HF Algorithm: Implementation, Optimised Auxiliary Basis Sets, Demonstration of Accuracy and Efficiency. *Phys. Chem. Chem. Phys.* **2002**, *4*, 4285−4291.
(40) Hättig, C. Optimization of Auxiliary Basis Sets for RI-MP2 and RI-CC2 Calculations: Core−valence and Quintuple-ζ Basis Sets for H to Ar and QZVPP Basis Sets for Li to Kr. *Phys. Chem. Chem. Phys.* **2005**, *7*, 59−66.
(41) Klopper, W. Highly Accurate Coupled-Cluster Singlet and Triplet Pair Energies from Explicitly Correlated Calculations in Comparison with Extrapolation Techniques. *Mol. Phys.* **2001**, *99*, 481−507.
(42) Youssaf, K. E.; Peterson, K. A. Optimized Auxiliary Basis Sets for Explicitly Correlated Methods. *J. Chem. Phys.* **2008**, *129*, 184108.
(43) Watts, J. D.; Gauss, J.; Bartlett, R. J. Coupled-Cluster Methods with Noniterative Triple Excitations for Restricted Open-Shell Hartree−Fock and other General Single Determinant Reference Functions. Energies and Analytical Gradients. *J. Chem. Phys.* **1993**, *98*, 8718−8733.
(44) Peterson, K. A.; Dunning, T. H. Accurate Correlation Consistent Basis Sets for Molecular Core−valence Correlation Effects: The Second Row Atoms Al−Ar, and the First Row Atoms B−Ne Revisited. *J. Chem. Phys.* **2002**, *117*, 10548−10560.
(45) Douglas, M.; Kroll, N. M. Quantum Electrodynamical Corrections to the Fine Structure of Helium. *Ann. Phys.* **1974**, *82*, 89−155.

DOI: 10.1021/acs.jpca.5b00466
J. Phys. Chem. A XXXX, XXX, XXX−XXX

(46) Jansen, G.; Hess, B. A. Revision of the Douglas-Kroll Transformation. *Phys. Rev. A* **1989**, *39*, 6016−6017.
(47) de Jong, W. A.; Harrison, R. J.; Dixon, D. A. Parallel Douglas−Kroll Energy and Gradients in NWChem: Estimating Scalar Relativistic Effects using Douglas−Kroll Contracted Basis Sets. *J. Chem. Phys.* **2001**, *114*, 48−53.
(48) Roca-Sanjuán, D.; Rubio, M.; Merchán, M.; Serrano-Andrés, L. *Ab initio* Determination of the Ionization Potentials of DNA and RNA Nucleobases. *J. Chem. Phys.* **2006**, *125*, 084302.
(49) Hudock, H. R.; Levine, B. G.; Thompson, A. L.; Satzger, H.; Townsend, D.; Gador, N.; Ullrich, S.; Stolow, A.; Martínez, T. J. Ab Initio Molecular Dynamics and Time-Resolved Photoelectron Spectroscopy of Electronically Excited Uracil and Thymine. *J. Phys. Chem. A* **2007**, *111*, 8500−8508.
(50) Calegari, F.; Ayuso, D.; Trabattoni, A.; Belshaw, L.; De Camillis, S.; Anumula, S.; Frassetto, F.; Poletto, L.; Palacios, A.; Decleva, P.; et al. Ultrafast Electron Dynamics in Phenylalanine Initiated by Attosecond Pulses. *Science* **2014**, *346*, 336−339.
(51) Furch, F. J.; Birkner, S.; Jungmann, J. H.; Kelkensberg, F.; Schulz, C. P.; Rouzée, A.; Vrakking, M. J. J. Photoelectron Imaging of XUV Photoionization of CO_2 by 13−40 eV Synchrotron Radiation. *J. Chem. Phys.* **2013**, *139*, 124309.

DOI: 10.1021/acs.jpca.5b00466
J. Phys. Chem. A XXXX, XXX, XXX−XXX